Spring 4-30-2021

Computational Study on Suppression of Airfoil Flow Separation using High-Frequency Translational Surface Actuation

Bibek Gupta

Computational Study on Suppression of Airfoil Flow Separation using High-Frequency Translational Surface Actuation

By
Bibek Gupta

A Thesis

submitted to the faculty of The University of Mississippi in partial fulfillment of the requirements of the Sally McDonnell Barksdale Honors College

The University of Mississippi
April 2021

Approved By

Advisor: Dr. Taiho Yeom

Reader: Dr. Wen Wu

Reader: Dr. Yiwei Han

ABSTRACT

Flow separation is a phenomenon that occurs when pressure increases in the streamwise direction of a flow, making a distinctive boundary layer or separation bubble. It causes aircraft to experience an increase in drag and noise and a decrease in a lift, hence degrading their aviation performance. This study uses numerical simulations to understand better the effects of high-frequency translational surface actuation (HFTSA) on flow separation control. The numerical simulations mimic the experimental parameters of an experiment performed by Okoye et al. on using the HFTSA system to control flow separation. A symmetrical airfoil structure of chord length of 0.3 m is drawn inside a computational domain with two velocity inlets and two pressure outlets. The velocity of streamwise flow is 4.3 m/s with the angle of attack -14 degrees. Structural grids of 946k nodes and 872k elements were generated for the computational domain. An actuation surface located on the suction surface of the airfoil uses User Defined Function to realize 122-micron mean-to-peak displacement with 565 Hz frequency. Large-eddy simulation turbulence model is adopted to capture vorticial structures within the airfoil wake. Velocity contours, pressure contours, velocity profiles, pressure profiles, and aerodynamic forces were examined before and after actuation. It is revealed that after actuation, the flow re-attaches, and separation bubbles were shrunk. After actuation, the lift coefficient increased by 180%, and the drag coefficient decreased by 28%. Hence, the HFTSA could suppress flow separation and improves aviation efficiency.

DEDICATION

I would like to dedicate this thesis to my loving parents, my dearest brother, and my sister. I also admire my friends on this journey. Their love and support have made me come so far and accomplish this work.

ACKNOWLEDGMENTS

I would like to thank and appreciate my advisor, Dr. Taiho Yeom, who has been phenomenal throughout this research project. He has nurtured me and taught me the research and writing process from zero levels. I would also like to extend my appreciation and gratitude to my advisory committee members, Dr. Wen Wu and Dr. Yiwei Han, for their valuable guidance and feedback throughout this research. Finally, I would like to express my huge thanks to my family and friends who have never failed to provide me care and support that I need the most. Their constructive and friendly environment always motivates me to push myself up and be a better person.

TABLE OF CONTENTS

LIST OF FIGURES

LIST OF TABLES

Introduction

An adverse pressure gradient is when the pressure increases in the streamwise direction of a flow, leading to flow separation and making a distinctive boundary layer. As an effect of adverse pressure gradient, reverse flow occurs at the downstream of separation, causing thickening of the boundary layer. Also, with the increase in the angle of the fluid's velocity, several reverse flow forms and flow separation get enlarged [1]. The flow separation largely affects aerodynamic performance, i.e., drag and lift. Also, during conditions like the high angle of attack (stall condition), take off/landing, and other flight conditions, separated or detached flow expands and affects important parameters of aerodynamic performance like drag and lift forces. Thus, the flow separation causes abrupt flow variation, increasing the drag and the moment of the flow system, causing inconsistent changes to aerodynamic fsorces [2].

Over the years, numerous studies and research have been done in flow separation control to improve aerodynamic efficiency. These studies have focused primarily on two types of flow control: passive flow control and active flow control. Passive flow control does not require any external energy sources; instead, it uses fixed geometry or geometrically shaped mechanical devices such as vortex generators to control the flow separation [3]. Vortex generators are generally a small vane attached to a lifting surface, designed to remove part of the slow-moving boundary layer near the wing surface, delaying the flow separation and the aerodynamic stalling.

A review study performed on low-profile vortex generators by Lin et al. suggests that low-profile vortex generators produce streamwise vortices which suppress the laminar separation bubble by energizing the near-wall laminar flow [4]. Prince et al. [5] performed experimental and computational study on flow control using a passive air-jet vortex generator. They found that a

spanwise array of passive air-jet vortex generators can increase lift coefficient and delay drag by effectively delaying trailing-edge separation and subsequent stall to higher angles of attack. Tejero et al. [6] used a passive rod vortex generator and studied its application on helicopter rotor blades using numerical simulations. They discovered that the rod vortex generator decreased the separation bubble's size and increased the aerodynamic efficiency of the rotor. Luo et al. [7] investigated a passive flow control strategy by installing a micro-cylinder near the suction surface of a stalled airfoil for high angles of attack. They found that the micro control device could diminish the separation region with smaller scales of vortices on the suction surface. Therefore, it improved the aerodynamic performance of the stalled airfoil.

Nevertheless, these benefits due to the control method were obtained at the loss of aerodynamic performance before stall, and its effectiveness got highly declined at an angle of attack greater than 22 degrees. Mohamed et al. [3] studied the application of bio-inspired nose on flow separation control. They modified the leading-edge profile of the airfoil to a nose design similar to cetacean species by creating a forward-facing step and a backward-facing step (cavity). This optimal nose-designed airfoil showed a 22.4 percent of maximum increase in aerodynamic efficiency. Zhou et al. [8] performed a computational study of the effects of Mach number on the passive control of flow separation by placing a small plate at the leading edge of an airfoil. This method creates a mutual interference between the trailing-edge vortex of the plate and the boundary layer of the airfoil. Using this method, they maintained a high lift coefficient of the airfoil with Mach numbers below 0.5, even at large angles of attack. However, it showed limited effectiveness for the flows over 0.5 Mach numbers. Due to difficulties associated with passive flow control, such as changing the profile of existing wings, positioning fixed vane vortex generators at different flow conditions, and drag penalties due to the installation of vortex

generators, active flow control methods have been proposed and studied. Active flow control techniques use external energy sources and are advantageous in terms of providing on-demand operation control.

Shan et al. [9] numerically explored active and passive flow control over a NACA0012 airfoil using vortex generators. Their investigation found out that passive vortex generators could reduce the separation zone by 80 percent. In contrast, the active vortex generator was proved to be more effective by making the separation zone invisible. Using a NACA 0015 wing and a synthetic jet actuator, Gilarranz et al. [10] explored flow separation control on the varying angle of attacks from -2.0 degree to 29.0 degrees. They discovered that the actuator had minimal effect on the flow separation for the angle of attacks lower than 10 degrees; however, the onset of the stall was successfully delayed at a higher angle of attacks. The synthetic jet actuator caused the increment of the stall angle by 6 degrees and the rise of the lift coefficient by 80 percent. The actuation was also able to decrease the drag on the wing. However, for the angle of attacks higher than 25 degrees, actuation with a larger frequency is required to affect the flow separation significantly. Melton [11] examined the momentum requirements of sweeping jet actuators for the flow separation control on a NACA 0015 Wing. It was found that a sweeping jet actuator with a high momentum coefficient is required for optimal performance when the actuator is placed downstream of the flow separation. Michelis et al. [12] found that the incoming disturbances from a dielectric barrier discharge plasma actuator caused shear layer breakdown of a laminar separation bubble.

Zong et al. [13] investigated the use of 26 plasma synthetic jet actuators on a NACA-0015 airfoil for controlling the leading-edge flow separation. Their study resulted that stall angle was increased from 15.5 degrees to 22 degrees, and the peak lift coefficient is increased by 21%. For the angle of attacks below 22 degrees, the flow separation control was found to be dependent on

the relative location of the actuation and separation and also on actuation frequency; however, frequency of the actuation did not affect the flow separation control for the angles of attack higher than 22 degrees. Kato et al. [14] used a plasma actuator driven by repetitive nanosecond pulse voltage to control flow separation. Their results show that the flow is steady, and the lift increment is independent of actuation frequency at the pre-stall and stall angles. However, the flow became unsteady at the post-stall angle and attained significant enhancement in the lift with the actuation.

These studies about active flow control using actuators give promising increment in aerodynamic efficiency and prompt in-depth studies in using different types of actuators, positioning the actuator and actuator frequency to produce optimal flow separation control.

Yeom et al. [15] explored improvements in the channel flow heat transfer due to piezoelectric translation actuation. Their results show a 55% enhancement in convection heat transfer coefficient. Okoye et al. [16] used a piezoelectric translational actuator which consisted of a piezoelectric stack actuator and an oval loop shell. The actuator could produce displacement of 0.1% and 0.15% of its length when a maximum AC voltage is applied with the help of the oval loop shell. They studied the effect of HFTSA on delaying the flow separation over an airfoil by performing a fog-based flow visualization experiment. They found that the flow separation was fully suppressed for the flow parameters of the 14-degree angle of attack, 4.3 m/s velocity, and 565 Hz frequency of the actuator.

This study replicates the flow conditions and flow separation control methods used by Okoye et al. [16] by using numerical simulation. Thus, it elaborates on the physical phenomenon and effect of the HFTSA on the suppression of flow separation and their aerodynamic forces.

2. EXPERIMENTAL PART

2.1 Experimental Setup

High-frequency translational surface actuation was realized by using a piezoelectric translational actuator (PTA). Figure 1 shows the schematics of the PTA used for the experiment. This PTA consists of a piezoelectric stack actuator and an oval loop structure. The actuation surface is 3D printed using PLA plastic, which is mounted on the top of the oval loop structure. Using the hole in the oval loop and fasteners, the PTA is anchored to the airfoil. The actuation surface is designed to blend with the airfoil surface and has a dimension of 62 mm (L_w) × 100 mm (L_a) with a 5 mm thickness. When an AC voltage is applied to the actuator, the stack actuator tends to produce small horizontal displacement, which then amplified to a vertical displacement by the oval loop structure.

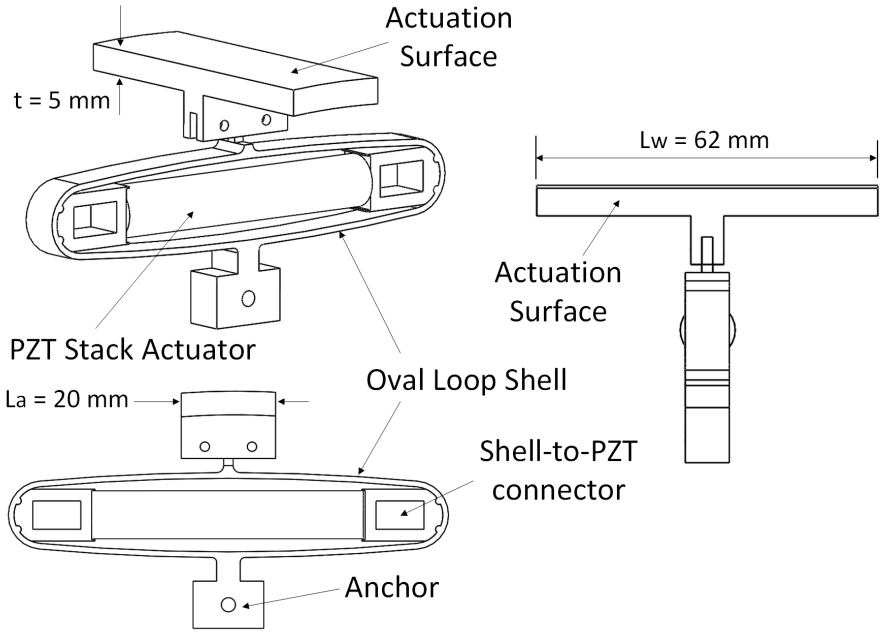

Figure 1. Schematics of a piezoelectric translational actuator (PTA) [16].

A symmetrical Eppler 862 airfoil with a spanwise length (L_s) and chord length (L_c) of 152.4 mm and 304.8 mm is used in the experiment. As shown in figure 2, the airfoil is designed

to have a removable suction surface for installing the HFTSA system inside the airfoil. The distance between the leading edges of the airfoil and the actuation surfaces is kept at 76.8 mm, about 25% of the chord length. A pivot point is installed at 50 mm from the leading edge of the airfoil to change the angle of attack (AoA).

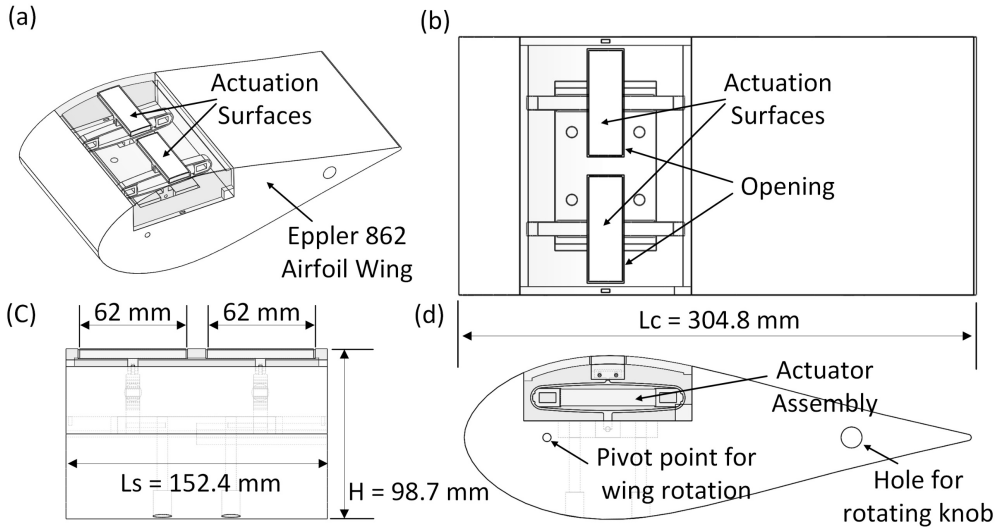

Figure 2. Wing assembly with high-frequency translational surface actuation (HFTSA) system: (a) iso-view, (b) top-view, (c) front-view, (d) side-view. [16].

Figure 4 shows the experimental setup of flow visualization experiments in a wind tunnel. The Pitsco X-Stream wind tunnel has a testing chamber of dimension 48.26 cm x 29.21 cm x 29.21 cm and a capacity of varying free stream velocity from 0 to 18 m/s. A wireless hot-wire digital anemometer was used to measure the free stream velocity. Using an Entour Ice fog generator, streams of dry ice fog were injected into the chamber from the inlet of the wind tunnel, and with the help of a continuous laser, the fog streams were illuminated. A high-speed Nikon 52 camera took sequential photographs of the airflow every 10 microseconds before and after the HFTSA

`

was turned on. Using the visualization pictures, flow separation control was analyzed for various conditions like free stream velocity, AoA, and HFTSA displacement.

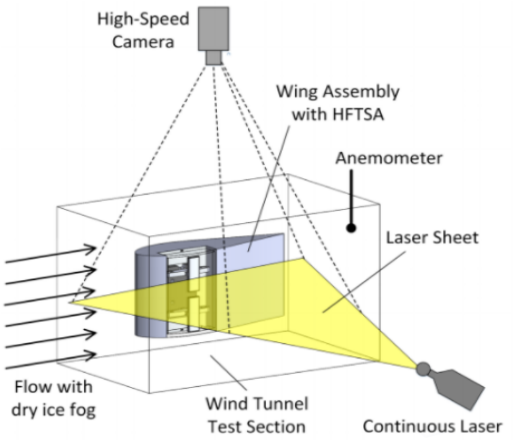

Figure 3. Experimental setup of flow visualization in a wind tunnel [16].

2.2 Experimental Results

The experiment was conducted for various flow and HFTSA parameters such as: for free stream velocities ($u\infty$) of 4.3 m/s, 8 m/s, and 12.7 m/s, for AoA of 0°, 6°, 12°, 14°, 18°, and 24°, and for mean to peak displacement of the actuator of 24 µm, 46 µm, 82 µm, and 122 µm. However, the optimal flow separation control was found when the free stream velocity was 4.3 m/s, for the airfoil having an AoA of 14° and the HFTSA system producing 122 µm mean-to-peak displacement with a frequency of 565 Hz.

Figures 4(a) and (b) show the wing structure at AoA = 14° and the relative positions of HFTSA leading edge (LE) and trailing edge (TE). Figures 4(c) and 4(d) are the flow visualization pictures captured at a particular instant time without and with the activation of HFTSA, respectively. It can be explicitly seen from figure 5(c) that there is a big separation bubble downstream of the flow separation point. However, when the HFTSA was turned on (figure 4(d)),

complete suppression of the separation bubble can be noticed. The results inferred that an optimal HFTSA system could delay or suppress the flow separation over the airfoil.

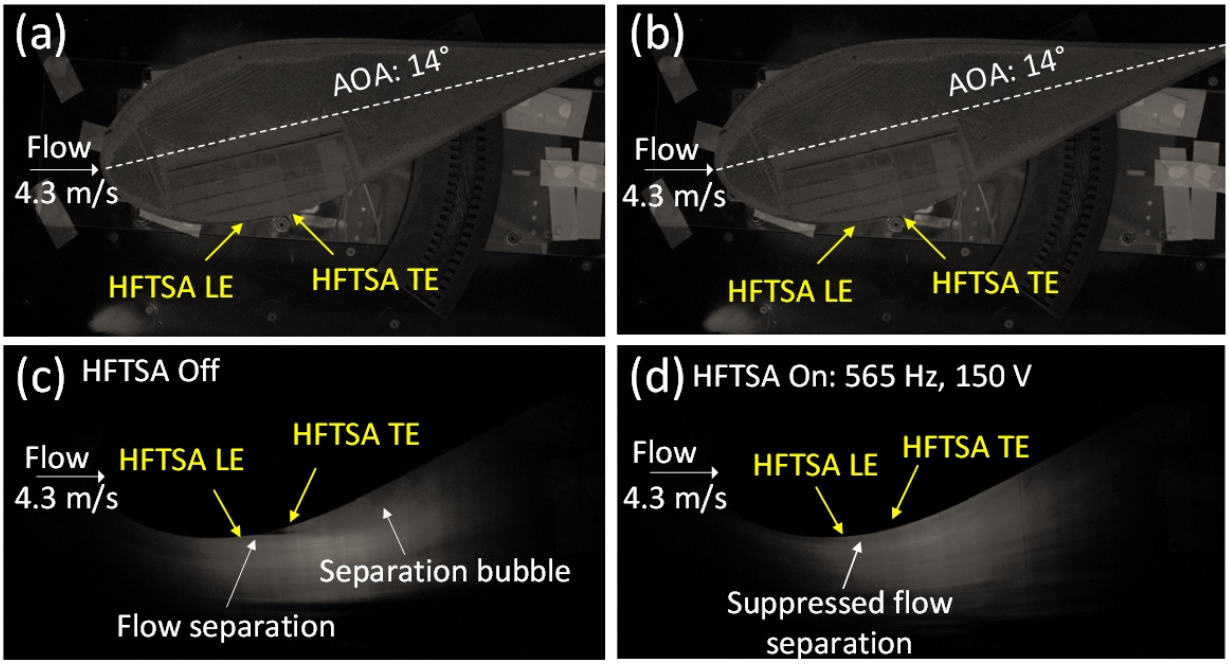

Figure 4. Validation of HFTSA on flow separation control at the specific condition of AOA = 14° with the maximum displacement: (a) and (b) references pictures of wing-assembly showing its relative positions and AOA with respect to the flow visualization photos; (c) flow visualization with the HFTSA off; (d) flow visualization with HFTSA on at 565 Hz and 150VAC [16].

3. NUMERICAL SIMULATIONS

Numerical simulations were performed to understand better the underlying physics of the effects of HFTSA on flow separation.

3.1 Computational Domain

The computational test case is asymmetric Eppler 862 airfoil with chord length (c = 0.3048 m) at AoA (α = -14˚) and Re = 88,700. As shown in figure 5, the computational domain covers 1c downstream, 1c in upstream, 1c in normal, and 0.1c in spanwise directions. A free stream with a

constant velocity of 4.3 m/s enters the domain from upstream and top boundaries. Downstream and bottom boundaries are set as pressure outlets with the ambient temperature.

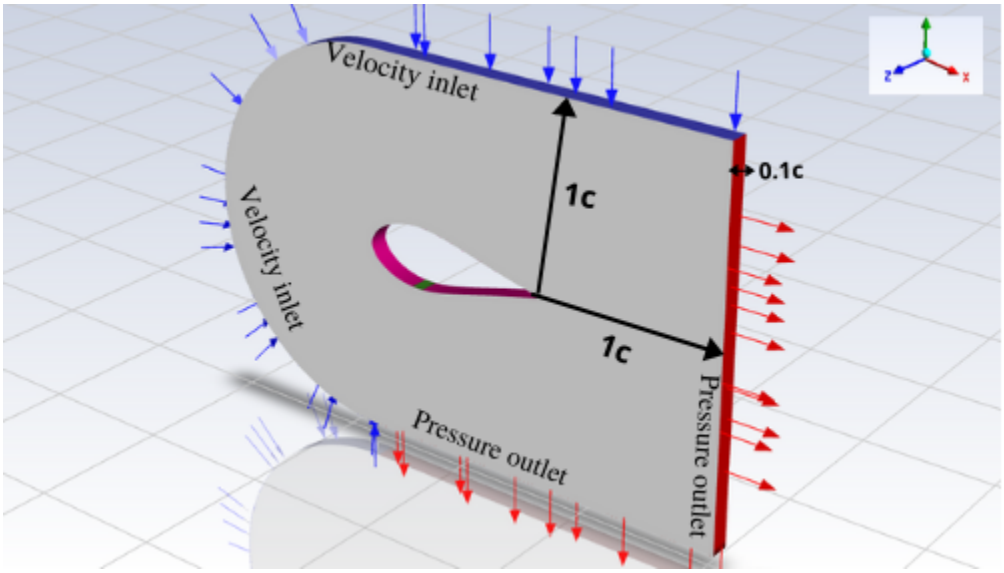

Figure 5. Computational domain and boundary conditions.

Figure 6 shows the computational airfoil geometry and the placement of the actuating surface. The leading edge of the actuation surfaces is aligned at a distance of 76.8 mm, which is about 25% of the chord length, from the airfoil's leading edge. The length of the actuation surface is 20 mm.

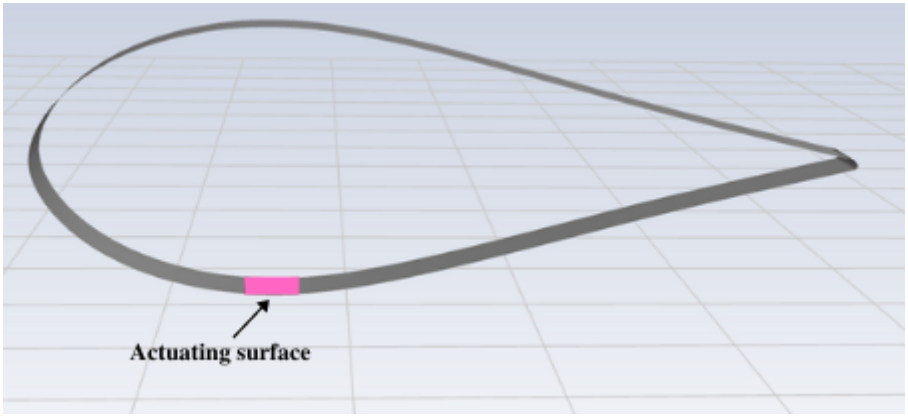

Figure 6. Positioning of actuation surface in the airfoi

`

3.2 Computational Grid

Structured grids were selected over unstructured grids since structured grids provide a high degree of quality and control to avoid numerical errors and get better convergence. The employed 872,781 hexahedron elements and 946,666 nodes. As seen in figure 7, the computational domain is partitioned to have more refined elements near the suction surface of the airfoil and coarser elements elsewhere to decrease computational time. The length of the elements of the airfoil surface is 1.75 x 10^{-4} m in the spanwise direction. The size of the elements near the suction surface of the airfoil is 1.5 x 10^{-3} m, while the maximum length of the grid is 1.0 x 10^{-2} m.

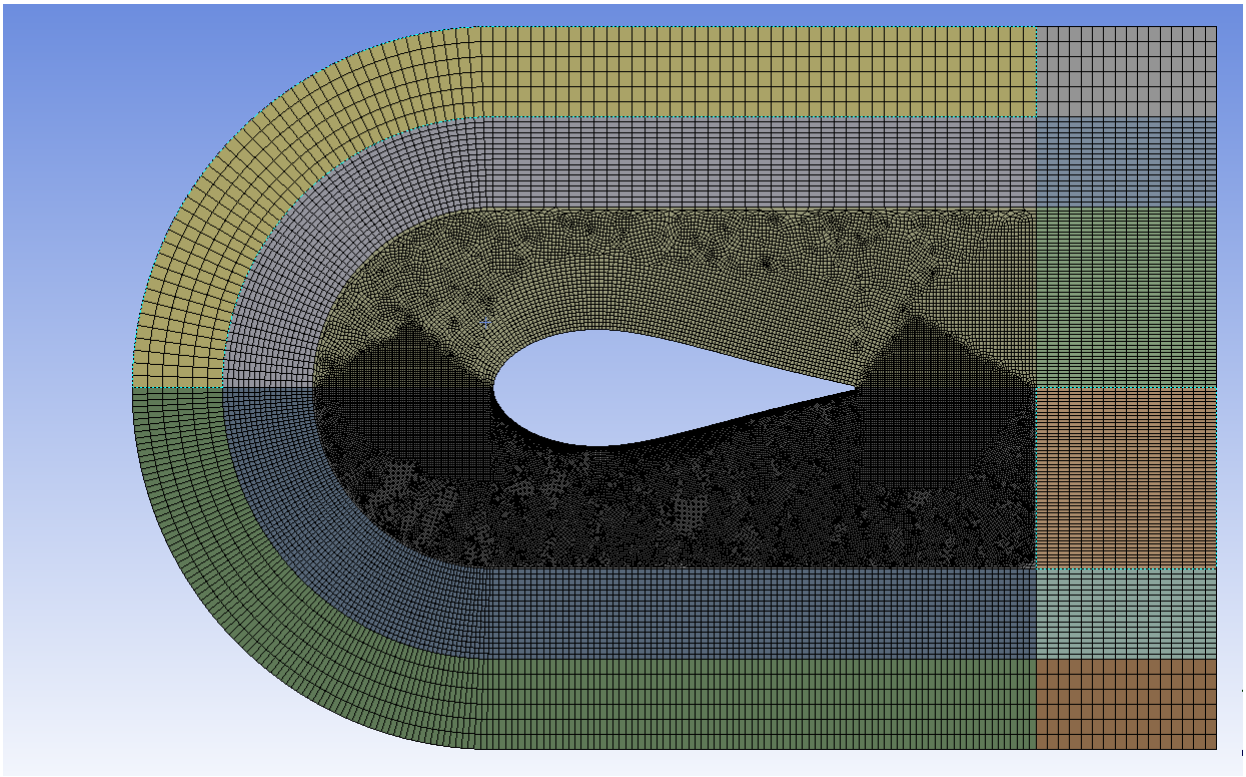

Figure 7**.** Computational grid of the entire domain.

`

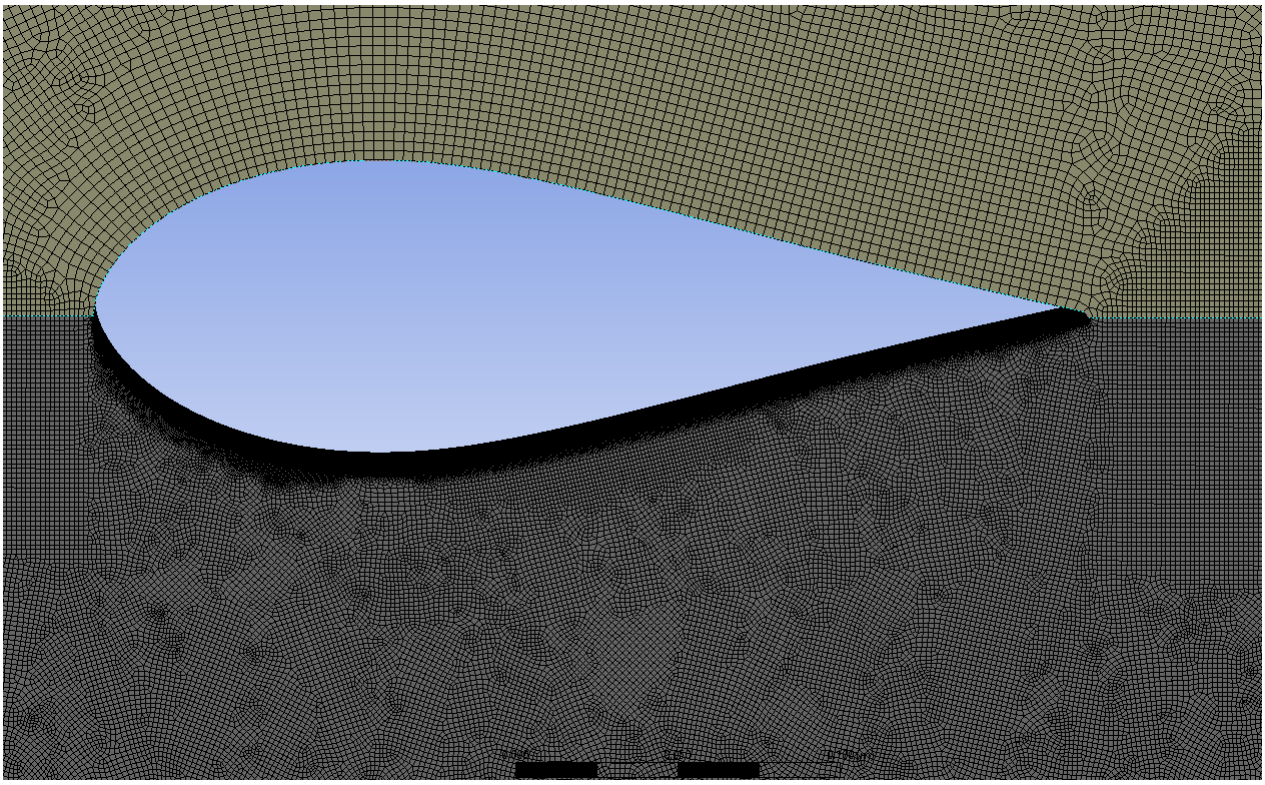

Figure 8. Close view of the computational grids near the airfoil surface.

3.3 Numerical Method Setup

All the simulations are performed with a pressure-based finite volume CFD solver for transient conditions. The governing equation are solved using a pressure-based coupled algorithm. The pressure equation is discretized spatially with the second order scheme whereas, the momentum equation has spatial discretization with bounded central differencing scheme. Bounded second-order implicit is used as transient formulations for the conditions without actuation condition, but for actuation turned on, transient formulations are set to first-order implicit. Adedoyin et al. [17] showed that Large Eddy Simulations (LES) with second-order discretization could predict turbulent structures very well and useful for these numerical simulations. The time step of the flow solver is set to 0.005 before actuation start and runs for 15s. However, after actuation, the time step size is 5.89 x 10^{-6} s to discretize the high frequency of the actuating

`

surface, and it runs for 0.43 s. High-frequency translational surface actuation (HFTSA) is realized by giving motion to the actuation surface of the airfoil using dynamic mesh features. User-defined function (UDF) - a programming code is used to realize the motion of the actuation surface. The following equation is used in the UDF with 565 Hz frequency and 122 x 10^{-6} m amplitude.

Equation 1:

Grid displacement = amplitude*2*3.141592*frequency*cos(2*pi*frequency*time)

4. RESULTS

4.1 Aerodynamic Performance Parameters of The Airfoil

The aerodynamic performance of the airfoil can be reflected by the parameters like lift and drag coefficients. The results are post-processed to get lift force and drag force. Figure 9 shows the resultant forces decomposed into force D parallel to the flow direction and force L perpendicular to the flow direction. The force L and D represent the lift and drag, respectively. Using equation 3 and 4, lift coefficient and drag coefficient are calculated before actuation and after actuation.

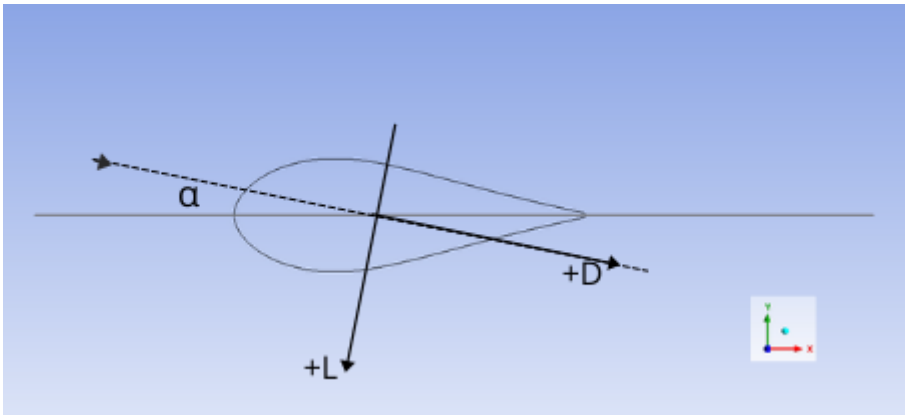

Figure 9. Schematic presentation of lift and drag

`

Equation 2: $$C_l = \frac{L}{\frac{1}{2}\rho v^2 c}$$

Equation 3: $$C_d = \frac{D}{\frac{1}{2}\rho v^2 c}$$

Where L is the lift; D is the drag; ρ is the density of the free stream; c is the chord length of the airfoil; v is the velocity of the free stream.

As shown in table 1, C_l and C_d are calculated to be 0.087 and 0.094, respectively, before actuation and 0.244 and 0.068, respectively, after actuation. Coefficient of lift increases by 180%, whereas the coefficient of drag decreases by 28%. These results confirm the positive effects of actuation on flow separation as it increases the aerodynamic efficiency of the airfoil.

Table 1: Percent changes in aerodynamic forces before and after actuation

Actuation Status	Drag Force	Lift force	C_d	C_l
Before Actuation	0.03134	0.0291	0.094	0.087
After Actuation	0.0227	0.0816	0.068	0.244
Percent Change	28% decrease	180% increase	28% decrease	180% increase

4.2 Velocity and Pressure Contours Before and After Actuation

In order to visualize the fluid flow and flow separation, x-component of velocity contours are plotted. Figure 10 shows a clear picture of the velocity field of the flow around the airfoil. Since the angle of attack is negative, the flow separation occurs downside of the airfoil. A distinctive boundary layer can be seen near the suction surface of the airfoil, which separates the

`

high-velocity field and low-velocity field. The large separation bubble, which are blue and pink regions in the contour, consists of very low-velocity fields and negative velocity fields. The negative velocity fields are reverse flows that occur due to increasing pressure downstream.

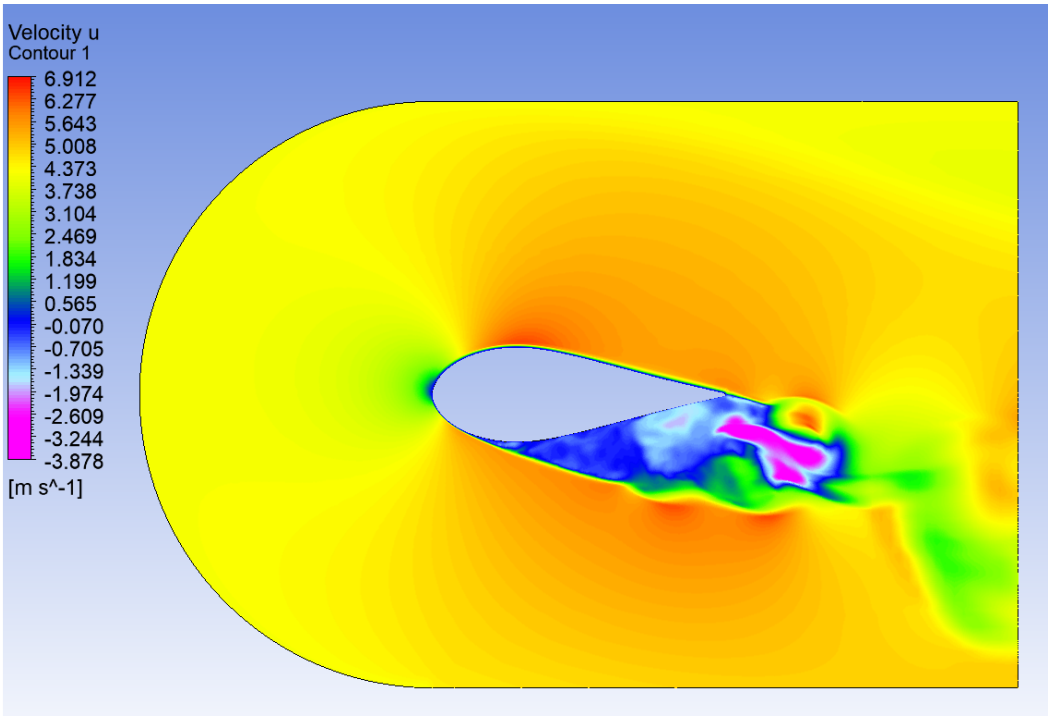

Figure 10. X-component velocity contour before actuation

Figure 11 demonstrates static pressure contours before actuation starts. The figure shows pressure gradients which are the main cause of the flow separation. The shear stress has a retarding effect upon the flow due to viscosity. Pressure is as high as 36 Pa near the trailing edge, causing the flow to retard or slow down. There is high pressure near the suction side of the airfoil than the upper side, resulting in lower flow velocity.

`

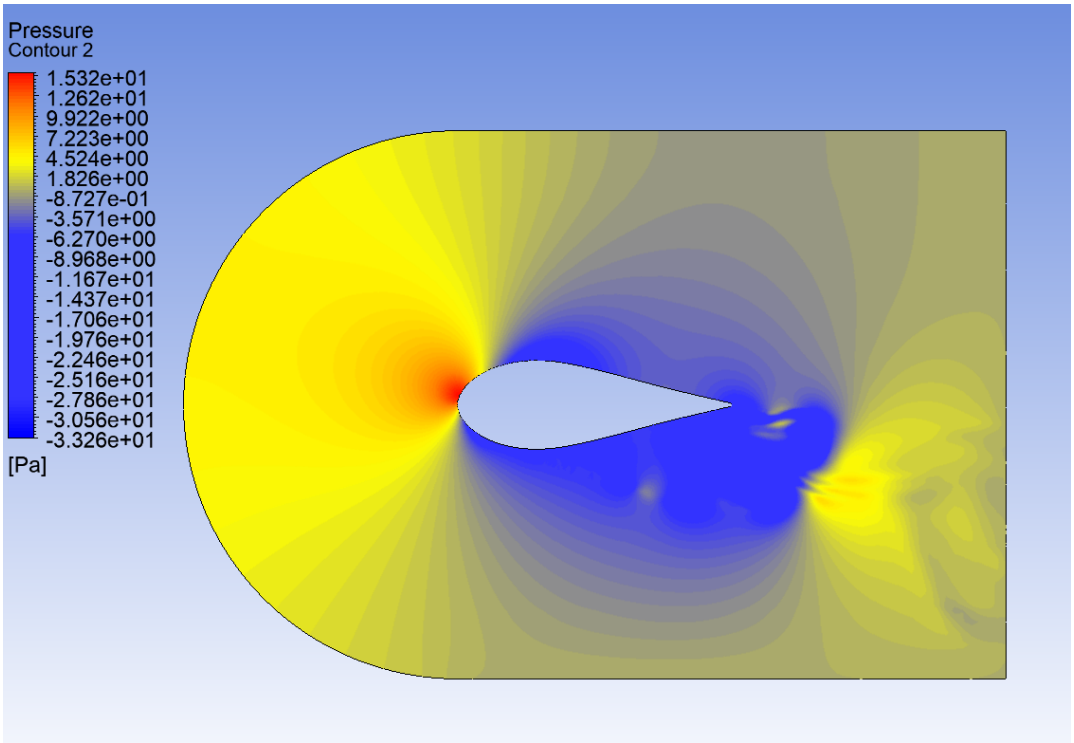

Figure 11. Static pressure contour before actuation

By introducing high-frequency translational surface actuation, the separation bubble has been diminished and become smaller, as demonstrated by figure 12. Some reverse flows still exist near the trailing edge, but it is comparatively less than before actuation. Figure 13 shows the lessening of large pressure gradients and the complete removal of negative pressure. The actuation is supposed to generate vortices that interfere with the boundary layer, bringing momentum and energy to the low-velocity region of the separation. This phenomenon is assisting in the reattachment of the boundary layer.

`

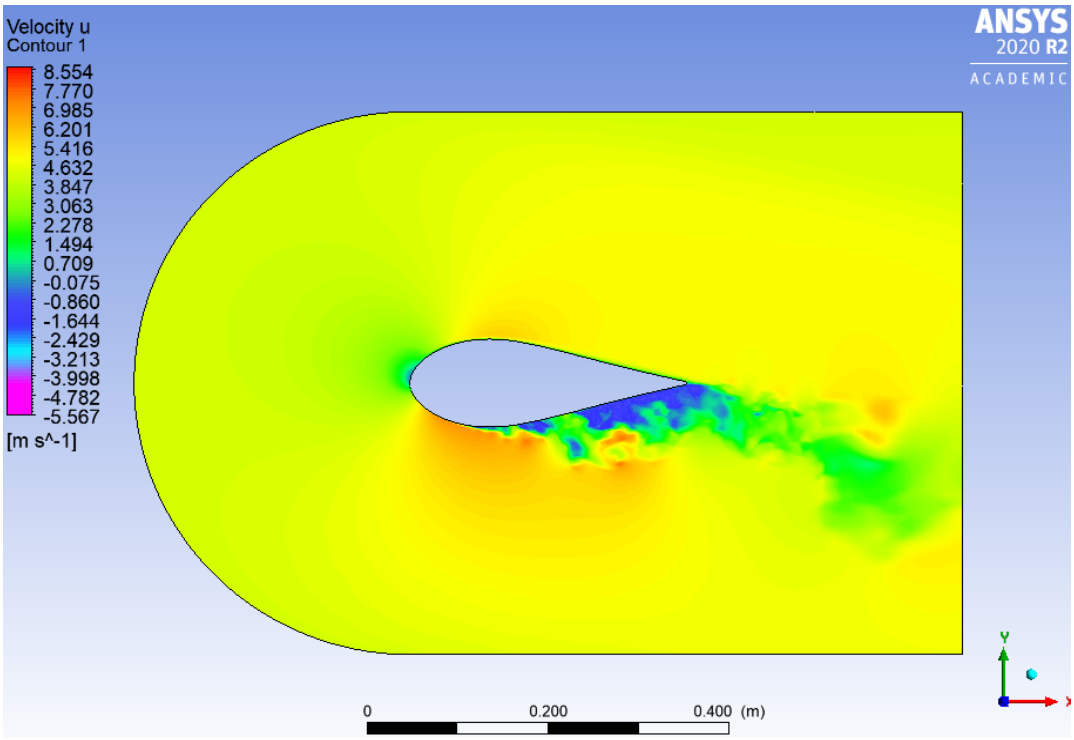

Figure 12. X-component velocity contour after actuation

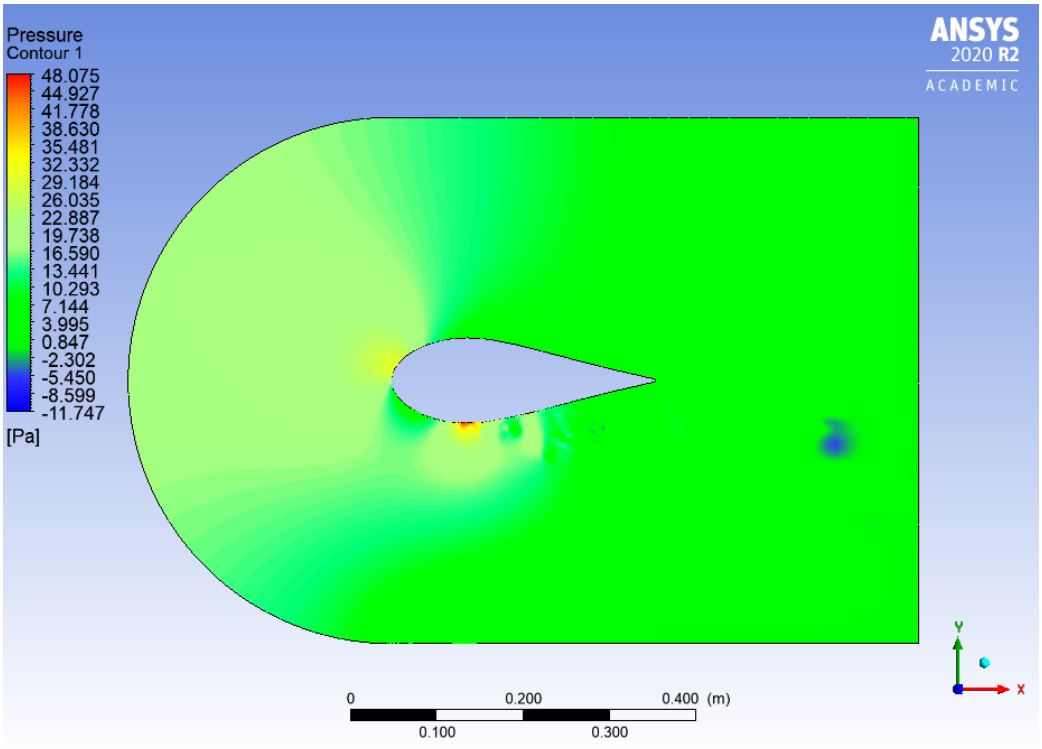

Figure 13. Static pressure contour after actuation

4.3 Time Averaged Velocity and Pressure Profiles

Eleven lines are drawn downside of the airfoil, as shown in figure 14. Velocity and pressure profiles are plotted along the line to show separation and reattachment clearly.

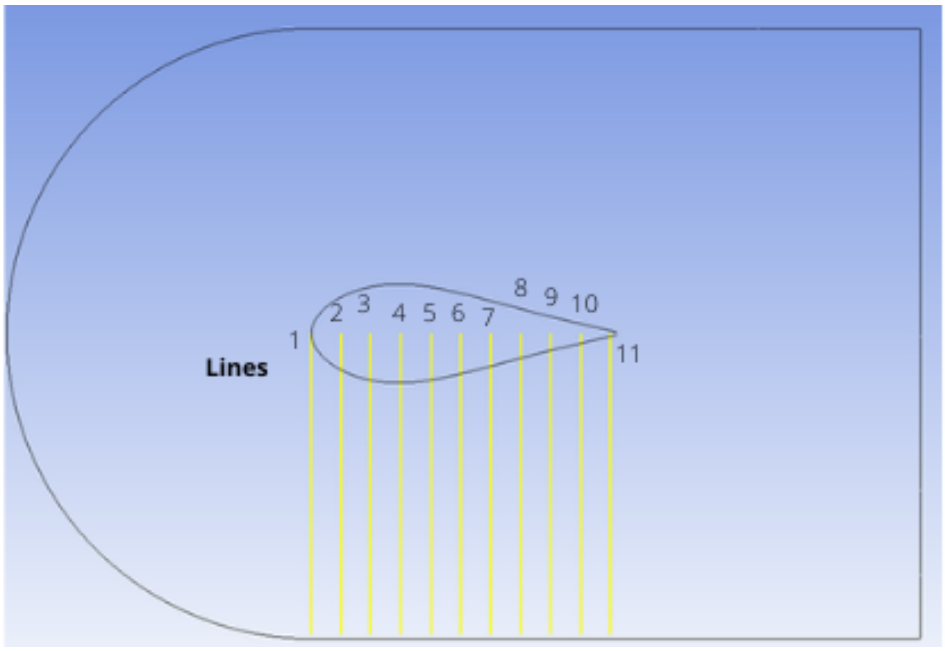

Figure 14. Representation of eleven lines for velocity and pressure profiles.

Each line has 500 points incorporated, and data values for pressure and velocity were recorded for 50 time-steps. The data points were averaged and plotted to get velocity and pressure profiles. The solid-black line, solid-red line, and dotted-magenta line represent data before actuation, after actuation, and a zero-line. Figure 15 illustrates that the flow velocity decreases, and reverse flows increase from the leading edge to the trailing edge near the airfoil surface. Negative velocity is seen in line 4, which explains that flow starts to separate somewhere near line 4, which is at 90 mm away from the airfoil's leading edge. Also, pressure values at all 11 lines are negative for the before actuation condition. However, due to the effect of HFTSA, the pressure

values are seen positive at all 11 lines. The velocity magnitude at the same points has increased, and even negative velocities are largely reduced.

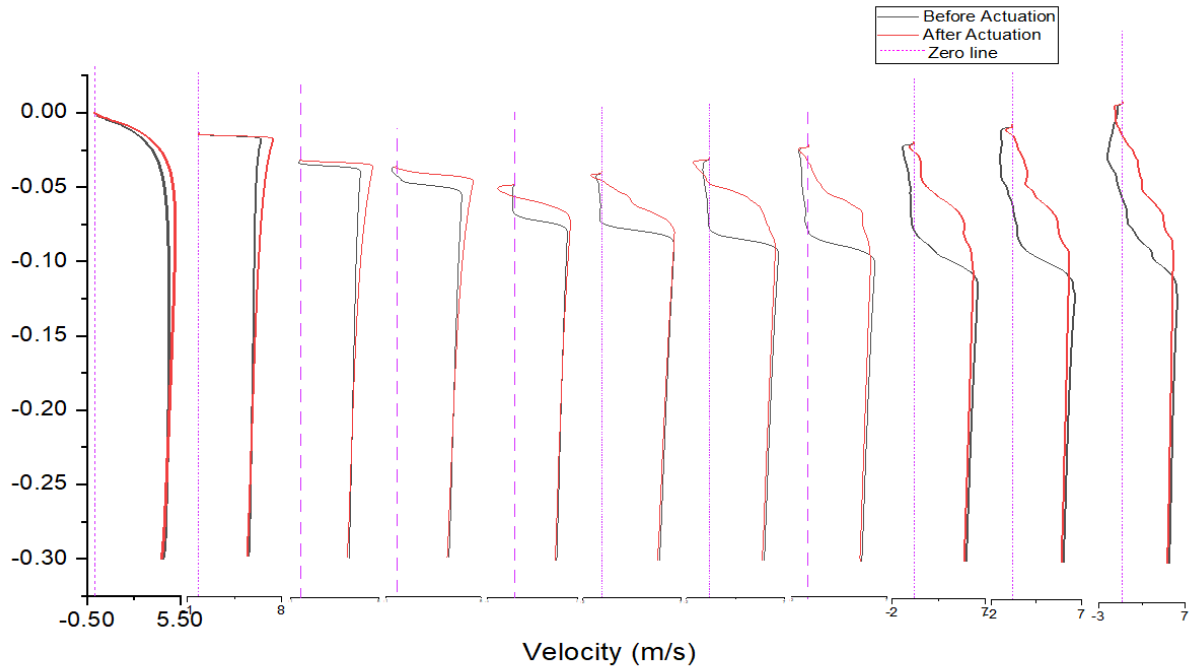

Figure 15. Velocity profiles at eleven lines before and after actuation

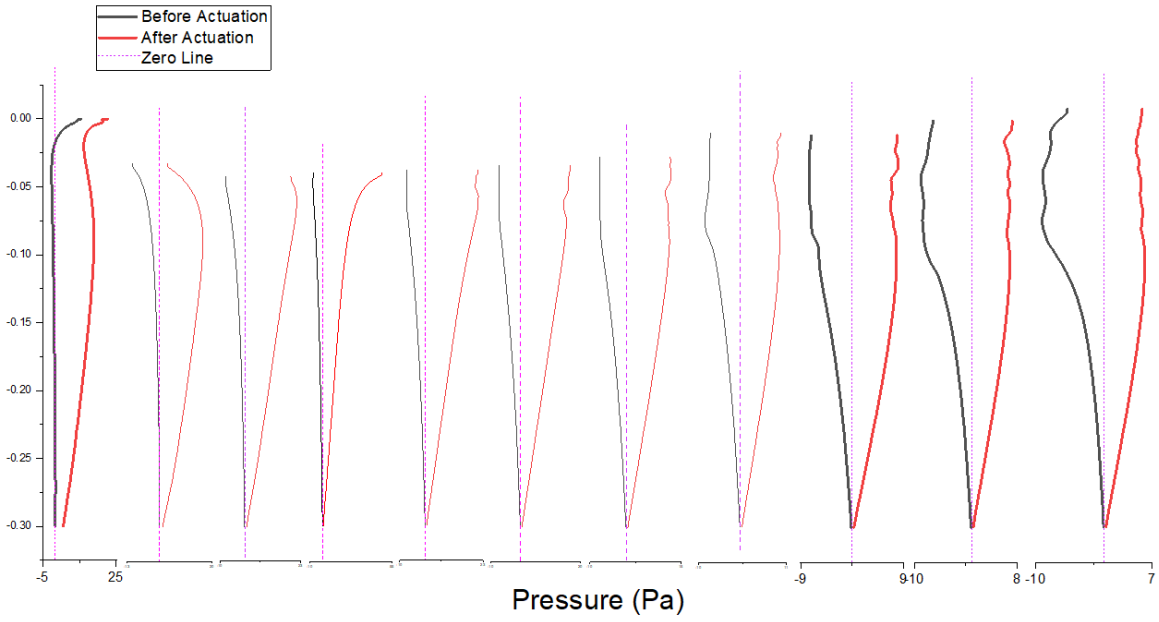

Figure 16. Pressure profiles at eleven lines before and after actuation

CONCLUSION AND RECOMMENDATION

Flow separation control using high-frequency translational actuation was investigated numerically. The numerical simulation is performed before and after high-frequency translational actuation for a symmetrical Eppler 862 airfoil with 0.3048 m chord and Re_c = 88,700 at $\alpha = 14°$. The actuation of the surface is realized by using a user-defined function with amplitude 122 x 10^{-6} m and 565 Hz frequency. The simulation is performed using the Large Eddy Simulation (LES) turbulence model, which has been proved to capture vortical structures and their effects. After evaluating the velocity and pressure contours of the flow field, it was evident that flow separation got suppressed, and the separation bubble also got reduced mainly after using the HFTSA mechanism. The simulation results agree with the experimental results performed by Okoye et al. This positive effect of HFTSA on flow separation caused a 180% increase in lift coefficient and decrease in drag coefficient by 28%, hence improving the aviation performance of the airfoil. Some future works could be beneficial, such as performing more experiments and simulations to investigate the effects of HFTSA on an airfoil at different parameters such as actuator location, frequency of actuation, the amplitude of actuation, angle of attacks, and incoming flow velocity.

REFERENCES

[1] Chang, P. K. (2014). Separation of flow. Elsevier.

[2] Ali, M. H., Mashud, M., Al Bari, A., & Islam, M. M. U. (2013). Aerodynamic drag reduction of a car by vortex generation. International Journal of Mechanical Engineering, 2(1), 12-21.

[3] Mohamed, M. A. R., Guven, U., & Yadav, R. (2019). Flow separation control of NACA-2412 airfoil with bio-inspired nose. Aircraft Engineering and Aerospace Technology.

[4] Lin, J. C. (2002). Review of research on low-profile vortex generators to control boundary-layer separation. Progress in Aerospace Sciences, 38(4-5), 389-420.

[5] Prince, S. A., Khodagolian, V., Singh, C., & Kokkalis, T. (2009). Aerodynamic stall suppression on aerofoil sections using passive air-jet vortex generators. AIAA journal, 47(9), 2232-2242.

[6] Tejero E, F., Doerffer, P., & Szulc, O. (2016). Application of a passive flow control device on helicopter rotor blades. Journal of the American Helicopter Society, 61(1), 1-13.

[7] Luo, D., Huang, D., & Sun, X. (2017). Passive flow control of a stalled airfoil using a microcylinder. Journal of Wind Engineering and Industrial Aerodynamics, 170, 256-273.

[8] Zhou, Y., Hou, L., & Huang, D. (2017). The effects of Mach number on the flow separation control of airfoil with a small plate near the leading edge. Computers & Fluids, 156, 274-282.

[9] Shan, H., Jiang, L., Liu, C., Love, M., & Maines, B. (2008). Numerical study of passive and active flow separation control over a NACA0012 airfoil. Computers & fluids, 37(8), 975-992.

[10] Gilarranz, J. L., Traub, L. W., & Rediniotis, O. K. (2005). A new class of synthetic jet actuators—part II: application to flow separation control. J. Fluids Eng., 127(2), 377-387.

[11] Pack Melton, L. G. (2014). Active flow separation control on a NACA 0015 wing using fluidic actuators. In 7th AIAA flow control conference (p. 2364).

[12] Michelis, T., Yarusevych, S., & Kotsonis, M. (2017). Response of a laminar separation bubble to impulsive forcing. J. Fluid Mech, 820, 633-666.

[13] Zong, H., van Pelt, T., & Kotsonis, M. (2018). Airfoil flow separation control with plasma synthetic jets at moderate Reynolds number. Experiments in Fluids, 59(11), 1-19.

[14] Kato, K., Breitsamter, C., & Obi, S. (2014). Flow separation control over a Gö 387 airfoil by nanosecond pulse-periodic discharge. Experiments in fluids, 55(8), 1-19.

[15] Yeom, T., Simon, T. W., Huang, L., North, M. T., & Cui, T. (2012). Piezoelectric translational agitation for enhancing forced-convection channel-flow heat transfer. International journal of heat and mass transfer, 55(25-26), 7398-7409.

[16] Okoye, K., Lai, W., & Yeom, T. (2020, November). Experimental Flow Visualization Study of Flow Separation Control With High-Frequency Translational Surface Actuation. In ASME International Mechanical Engineering Congress and Exposition (Vol. 84515, p. V004T04A002). American Society of Mechanical Engineers.

[17] Adedoyin, A. A., Walters, D. K., & Bhushan, S. (2015). Investigation of turbulence model and numerical scheme combinations for practical finite-volume large eddy simulations. Engineering Applications of Computational Fluid Mechanics, 9(1), 324-342.